Composites: Part A 72 (2015) 239–248

Contents lists available at ScienceDirect

Composites: Part A

journal homepage: www.elsevier.com/locate/compositesa

The stiffness tensor for composites with curved discontinuous fibers

Vlastimil Kunc [a,*], Scott W. Case [b], Hector J. Santos-Villalobos [a], Srdjan Simunovic [a]

[a] Oak Ridge National Laboratory, PO Box 2008, MS6053, Oak Ridge, TN 37831-6053, USA
[b] Virginia Polytechnic Institute and State University, Engineering Science and Mechanics, 225-A Norris Hall, Blacksburg, VA 24061, USA

ARTICLE INFO

Article history:
Available online 5 June 2014

Keywords:
B. Mechanical properties
C. Anisotropy
B. Modeling
Micro-mechanics

ABSTRACT

In this paper, we propose a new method for calculating the stiffness tensor for a composite material containing curved discontinuous fibers. We introduce a new concept of configuration for a single curved fiber defined by five dimensionless parameters. An ensemble of curved fibers within a composite material is then described by a configuration probability density function. The proposed stiffness tensor requires three tensors of fourth-order describing the material microstructure and a set of elastic constants. We introduce the concept of configuration averaging and present an analytical method for estimating elastic constants for materials containing curved fibers. We demonstrate that for materials containing only straight fibers, fiber configuration and configuration averaging reduces to standard fiber orientation and orientation averaging. Comparison of stiffness measurements using X-ray digital image correlation against the stiffness calculated with fiber geometry obtained by X-ray tomography shows that accounting for fiber curvature provides better estimate of stiffness.

© 2014 Elsevier Ltd. All rights reserved.

1. Introduction

Discontinuous fiber reinforced composites (DFCs) are materials in which the fibers act as structural reinforcements and their aspect ratios, defined as fiber length divided by fiber diameter, influence the resulting material properties. Examples of traditional production processes for DFCs are injection molding, compression molding, and spray-up. However, this work can be applied equally well to metal matrix composites and bio-composites. The work presented below assumes linear elastic matrix properties, therefore applications should focus on materials obeying this assumption until extentions of the method are introduced to remove this restriction. The objective of this work was to develop an improved description of microstructure of DFCs that accounts for curved fibers and to develop a method for obtaining the stiffness tensor of the composite. Since material stiffness is a common design driver, this work also provides a practical design tool.

In developing this work, we acknowledge that virtually any microstructure can be explicitely modeled using numerical techniques such the finite element method (FEM) [1,2]. However, an obvious disadvantage of this approach is the need to generate a large, statistically significant number of representative volumes for quasi-random architectures and to subsequently perform analyses on all of them in order to obtain the statistics of the resulting response. Modeling of realistic DFCs using such an approach would require prohibitive computer resources and time.

An alternative modeling approach is to use statistical measures and homogenization methods for describing the fiber and matrix microstructure in the representative volumes of the composite. These measures and methods are largely driven by the nature of the subsequent analysis. The microstructure measures commonly used for composite stiffness prediction are fiber volume fraction, fiber length distribution (FLD), and fiber orientation distribution (FOD). Fiber volume fraction is a single parameter describing an average content of fiber and matrix material within the composite. FLD and FOD are functions describing an ensemble of fibers, represented as straight cylinders. Measurement techniques and results for traditional flow molded DFCs are discussed for example in [3–5] for FLD, [6,7] for FOD and standards [8,9] covering fiber volume fraction.

The orientation of a single straight fiber is described by an orientation vector. The probability density function (PDF) describing the orientation for an ensemble of fibers can be represented by a set of even order orientation tensors as described in [10]. Using a fourth order orientation tensor and the micromechanics-based material stiffness coefficients, Advani and Tucker [10] obtain the stiffness tensor using orientation averaging of transversely isotropic stiffness tensor.

In this work, we extend the work of Advani and Tucker for composites containing straight fibers with arbitrary orientation [10] to

* Corresponding author. Tel.: +1 865 919 4595; fax: +1 865 574 8257.
E-mail addresses: kuncv@ornl.gov (V. Kunc), scase@vt.edu (S.W. Case), hsantos@ornl.gov (H.J. Santos-Villalobos), simunovics@ornl.gov (S. Simunovic).

http://dx.doi.org/10.1016/j.compositesa.2014.05.018
1359-835X/© 2014 Elsevier Ltd. All rights reserved.

composites containing assemblies of curved fibers. The resulting stiffness tensor is anisotropic. This extension is motivated by experimental observations such as that shown in Fig. 1.

In order to systematically account for the effect of fiber curvature on the composite properties, we introduce a new concept of fiber configuration and a PDF for the configuration of the ensemble of fibers. We then introduce a method of configuration averaging of the orthotropic stiffness tensor that results in a stiffness tensor containing 21 distinct components. To obtain numerical values of the material constants for the orthotropic stiffness tensor, we use the Halpin-Tsai equations [11] along with orientation averaging (although these constants could be generated by other methods). Finally, we demonstrate the developed method with examples.

2. Description of microstructure

2.1. Configuration of single fiber

The first step in our approach is to introduce the configuration description for a single curved fiber. We define a fiber coordinate system **f** = (**p**, **q**, **s**) as a Cartesian coordinate system defined by orthonormal vectors **p**, **q**, and **s**. We assume a straight cylindrical fiber of length L and diameter d and place it so that the center of gravity of the fiber coincides with the origin of the fiber coordinate system and the fiber centerline is parallel to **p** as shown in Fig. 2.

The fiber configuration is then defined by a single dimensionless parameter $\xi = \frac{L}{d}$ and orientation vector (1,0,0) in coordinate system **f**.

Four successive geometry transformations will result in a curved fiber in a general configuration with respect to a laboratory coordinate system. These operations consist of first changing the fiber from a straight to a curved shape and then rotating it using three Euler angles. We then change the shape of the fiber so that the oriented curvature ρ is given by $\boldsymbol{\rho} = \frac{1}{R}\boldsymbol{q}$, where R is the radius of curvature. This is equivalent to describing a section of a toroid in cylindrical coordinates $(r, \varphi, \bar{z})$ with cylindrical coordinate system origin at R**q**, $\bar{z}$ axis aligned with **s** and φ measured from $\bar{x}$ in a mathematically positive sense as shown in Fig. 2, right.

We assume that the fiber length and diameter remain the same, and the vector **p** remains tangent to the fiber centerline at its center. This fiber configuration is given by two dimensionless parameters, $\xi = \frac{L}{d}$ and $\eta = \frac{L}{R}$. We further assume that the fiber coordinates f_i are initially aligned with the laboratory coordinates x_i and perform three successive rotations through three Euler angles: rotation around **s** by α, rotation around **q** by β, and rotation around **p** by γ in mathematically positive sense. These operations are described by

$$f_l = R^x_{kl} R^y_{jk} R^z_{ij} x_i \quad i,j,k,l = 1,2,3 \tag{1}$$

In (1) and all subsequent equations in this document, summation takes place over repeated indices unless otherwise noted. The direction cosines in (1) are given by

$$R^x_{kl} = \begin{bmatrix} 1 & 0 & 0 \\ 0 & \cos\gamma & \sin\gamma \\ 0 & -\sin\gamma & \cos\gamma \end{bmatrix}, \quad R^y_{jk} = \begin{bmatrix} \cos\beta & 0 & \sin\beta \\ 0 & 1 & 0 \\ -\sin\beta & 0 & \cos\beta \end{bmatrix}, \quad R^z_{ij} = \begin{bmatrix} \cos\alpha & \sin\alpha & 0 \\ -\sin\alpha & \cos\alpha & 0 \\ 0 & 0 & 1 \end{bmatrix} \tag{2}$$

We may obtain a unique description of a curved fiber in any configuration by placing the following limits on the rotations:

$$0 \le \alpha < 2\pi; \quad -\frac{\pi}{2} \le \beta < \frac{\pi}{2}; \quad 0 \le \gamma < 2\pi \tag{3}$$

Therefore, the configuration of a curved fiber can be described by five dimensionless parameters $\xi, \eta, \alpha, \beta, \gamma$ as illustrated in Fig. 3. Parameters ξ, η describe the shape of the curved fiber, while the three angles α, β, γ allow for arbitrary rotation of this shape with respect to the laboratory coordinates.

Note that the limiting case of a straight fiber ($\eta = 0$) reduces to the coordinate system of Advani-Tucker [10] (with spherical coordinate angles $\phi = \alpha$, $\theta = \frac{\pi}{2} - \beta$) where γ can be selected arbitrarily without affecting the configuration state. The components of the orientation vector **p** and the curvature vector **q** are:

$$p_1 = \cos\alpha\cos\beta = \cos\phi\sin\theta; \quad p_2 = \sin\alpha\cos\beta = \sin\phi\sin\theta; \quad p_3 = \sin\beta = \cos\theta \tag{4}$$

$$q_1 = -\sin\alpha\cos\gamma - \cos\alpha\sin\beta\sin\gamma; \quad q_2 = \cos\alpha\cos\gamma - \sin\alpha\sin\beta\sin\gamma; \quad q_3 = \cos\beta\sin\gamma \tag{5}$$

The configuration of a straight fiber is described by three parameters, namely the aspect ratio $\xi = \frac{L}{d}$ and two angles defining the orientation of fiber vector **p**. Eq. (4) gives the orientation vector components with Euler angles α, β as well as with standard spherical coordinate angles ϕ, θ to allow for easy comparison with previously published work [10]. The description of configuration for a curved fiber requires one additional shape parameter and one additional angle. The shape parameter $\eta = \frac{L}{R}$ provides the magnitude of curvature, while the angle γ provides the direction of the curvature vector **q**, which is by definition perpendicular to the orientation vector **p**.

2.2. Configuration distribution function for an ensemble of fibers

We now define the configuration distribution function for an ensemble of fibers $\psi_C(\alpha, \beta, \gamma, \xi, \eta)$ as the probability density function of finding a fiber with configuration given by angles and parameters $\alpha, \beta, \gamma, \xi, \eta$ in the intervals:

$$\begin{aligned} P(&\alpha_1 \le \alpha \le \alpha_1 + d\alpha_1, \beta_1 \le \beta \le \beta_1 + d\beta_1, \gamma_1 \le \gamma \le \gamma_1 + d\gamma_1, \xi_1 \\ &\le \xi \le +\xi_1 + d\xi_1, \eta_1 \le \eta \le +\eta_1 + d\eta_1) \\ &= \psi(\alpha_1, \beta_1, \gamma_1, \xi_1, \eta_1)\cos\beta_1 \quad d\alpha d\beta d\gamma d\xi d\eta \end{aligned} \tag{6}$$

The configuration distribution function ψ is normalized as:

$$\int_{\eta=0}^{\infty}\int_{\xi=0}^{\infty}\int_{\gamma=0}^{2\pi}\int_{\beta=-\pi/2}^{\pi/2}\int_{\alpha=0}^{2\pi}\psi_C(\alpha,\beta,\gamma,\xi,\eta)\cos\beta \quad d\alpha d\beta d\gamma d\xi d\eta = 1 \tag{7}$$

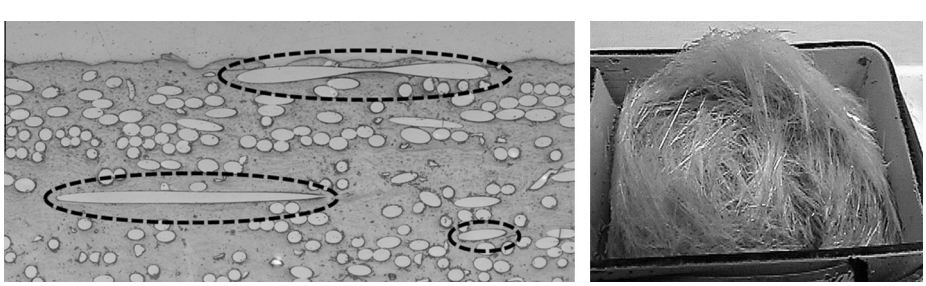

Fig. 1. Injection molded composite containing glass fibers. Left: Polished cross-section – three cross-sections whose deviation from elliptical shape indicates fiber curvature are highlighted. Right: Entangled mass of curved fibers after matrix burn-off.

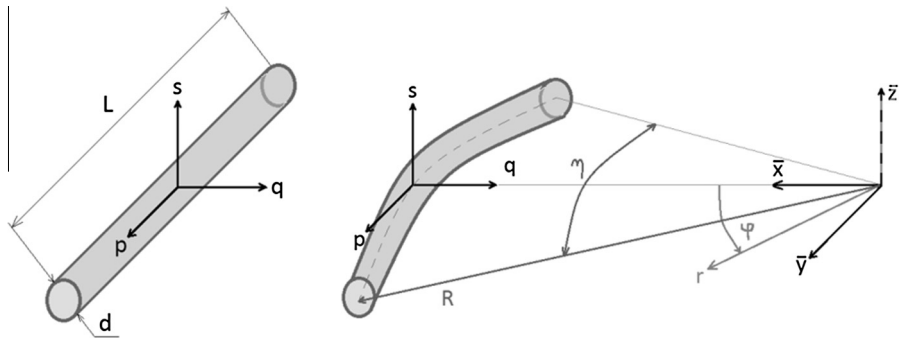

Fig. 2. Left: Straight cylindrical fiber with coordinate system **f** = (**p**, **q**, **s**). Right: Bent fiber with curvature radius R.

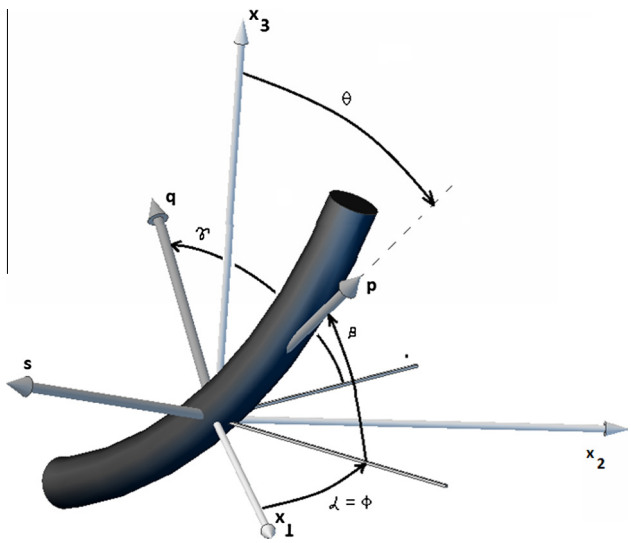

Fig. 3. Curved fiber with coordinate system **f** = (**p**, **q**, **s**), defined by Euler angles α, β, γ. (For interpretation of the references to color in this figure legend, the reader is referred to the web version of this article.)

Assuming the independence of fiber shape and rotation, ψ may be separated into two parts

$$\psi_C(\alpha,\beta,\gamma,\xi,\eta) = \psi_R(\alpha,\beta,\gamma)\psi_S(\xi,\eta) \tag{8}$$

where the rotation of fiber coordinate system with respect to laboratory system given by three angles α, β, γ and the shape of a fiber given by parameters ξ, η are independent for an arbitrary configuration. We place the following normalization conditions on the rotation distribution function ψ_R and the shape distribution function ψ_S

$$\int_{\gamma=0}^{2\pi}\int_{\beta=-\pi/2}^{\pi/2}\int_{\alpha=0}^{2\pi}\psi_R(\alpha,\beta,\gamma)\cos\beta \quad d\alpha d\beta d\gamma = 1;$$
$$\int_{\eta=0}^{\infty}\int_{\xi=0}^{\infty}\psi_S(\xi,\eta)d\xi d\eta = 1 \tag{9}$$

Upon integration of ψ_R over all possible angles γ, the fiber orientation distribution function is:

$$\psi(\alpha,\beta) = \int_{\gamma=0}^{2\pi}\psi_R(\alpha,\beta,\gamma)d\gamma \tag{10}$$

The properties of ψ were explored in detail by Advani and Tucker [10].

2.3. Stiffness tensor

In this section, we use the concept of fiber configuration to establish the components of the anisotropic stiffness tensor C_{ijkl} for an ensemble of fibers in an arbitrary configuration. The generalized Hooke's law is given by

$$\sigma_{ij} = C_{ijkl}\varepsilon_{kl} \quad i,j,k,l = 1,2,3 \tag{11}$$

where σ_{ij} and ε_{kl} are the components of symmetric second rank stress and strain tensors respectively. Assuming the existence of a strain energy density function and the symmetry of the stress and strain tensors, we note the following (standard) symmetry of the stiffness tensor

$$C_{ijkl} = C_{jikl} = C_{klij} = C_{ijlk} \quad i,j,k,l = 1,2,3 \tag{12}$$

which reduces the number of distinct components in C_{ijkl} from 81 to 21. In the following sections, our focus is on deriving these 21 components of C_{ijkl} for any material with its microstructure described by Eq. (8).

2.4. Orthotropic stiffness tensor for a material with fibers in a single configuration

We now consider a material consisting of an ensemble of uniformly dispersed fibers of a single configuration within a matrix with no interactions between the fibers as illustrated in Fig. 4.

For the material illustrated in Fig. 4, a single fiber and surrounding matrix shown in Fig. 3 constitutes a representative volume. We can inspect Fig. 3 and conclude that there exists geometrical symmetry with respect to a plane with normal **p** and to a plane with normal **s**. Since our idealized material consists of fibers in a single configuration, the resulting material will also have two material planes of symmetry. We can write two transformations under which a stiffness tensor remains invariant

$$R_{ij}(\mathbf{p}) = \delta_{ij} - p_i p_j \text{ and } R_{ij}(\mathbf{s}) = \delta_{ij} - s_i s_j \quad i,j = 1,2,3 \tag{13}$$

Vectors **p** and **s** are normal; this was shown to imply a third material plane of symmetry [12] and result in orthotropic material stiffness tensor $\widetilde{C}_{ijkl}$ with nine material constants

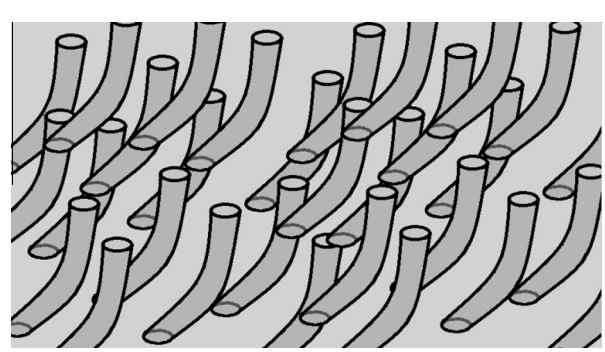

Fig. 4. Material with fibers in single configuration.

$$\begin{aligned}\widetilde{C}_{ijkl} =& \mu(\delta_{ik}\delta_{jl}+\delta_{il}\delta_{jk})+\lambda\delta_{ij}\delta_{kl}+\kappa_{p2}(p_ip_j\delta_{kl}+\delta_{ij}p_kp_l)\\ &+\kappa_{q2}(q_iq_j\delta_{kl}+\delta_{ij}q_kq_l)+2\mu_1(\delta_{ik}p_jp_l+\delta_{il}p_jp_k+\delta_{jl}p_ip_k+\delta_{jk}p_ip_l)\\ &+2\mu_2(\delta_{ik}q_jq_l+\delta_{il}q_jq_k+\delta_{jl}q_iq_k+\delta_{jk}q_iq_l)+\kappa_{p4}p_ip_jp_kp_l\\ &+\kappa_{q4}q_iq_jq_kq_l+\kappa_{s4}(p_ip_jq_kq_l+q_iq_jp_kp_l)\quad i,j,k,l=1,2,3 \end{aligned} \tag{14}$$

This form of orthotropic stiffness tensor can be found for example in [13] and [14]. Spencer [14] also suggested that the vectors **p** and **q** may vary point to point for a material containing curved fibers. We extend this idea by introducing the concept of configuration averaging in a representative volume.

2.5. Configuration averaging for a material with an arbitrary fiber configuration

We now perform configuration averaging to obtain the stiffness tensor for material containing fibers described by a configuration distribution function ψ. This procedure is analogous to orientation averaging. We define the configuration average of the stiffness tensor as

$$\begin{aligned}\langle C_{ijkl}\rangle_C =& \int_{\eta=0}^{\infty}\int_{\xi=0}^{\infty}\int_{\gamma=0}^{2\pi}\int_{\beta=-\pi/2}^{\pi/2}\int_{\alpha=0}^{2\pi}\widetilde{C}_{ijkl}\psi_C(\alpha,\beta,\gamma,\xi,\eta)\\ &\times\cos\beta\quad d\alpha d\beta d\gamma d\xi d\eta\quad i,j,k,l=1,2,3\end{aligned} \tag{15}$$

where we use $\langle\rangle_c$ brackets to indicate configuration averaging. Substituting Eqs. (14) into (15) results in the most general form of a stiffness tensor for material containing curved fibers. We now use the standard separation of variables in Eq. (8) to describe independence of fiber shape and its rotation with respect to the laboratory system. This allows us to simplify configuration averaging (15) by separating rotation averaging and shape averaging as discussed below.

The material constants in Eq. (14) are independent of the orientation of the fiber coordinate system with respect to laboratory system. However, they depend on parameters ξ and η for a particular configuration. Therefore for any of the material constants k (with units of Pa) of Eq. (14)$k = k(\xi, \eta)$.

Since the orientation vector **p** for any configuration is obtained by two rotations through angles α, β and the curvature vector **q** is then obtained by additional rotation around orientation vector **p** through angle γ, we can write

$$\mathbf{p}=\mathbf{p}(\alpha,\beta);\quad \mathbf{q}=\mathbf{q}(\alpha,\beta,\gamma) \tag{16}$$

Performing the requisite integration, Eq. (15) becomes

$$\begin{aligned}\langle C_{ijkl}\rangle_C =& \bar{\mu}(\delta_{ik}\delta_{jl}+\delta_{il}\delta_{jk})+\bar{\lambda}\delta_{ij}\delta_{kl}+\overline{\kappa_{p2}}(a_{ij}\delta_{kl}+\delta_{ij}a_{kl})\\ &+\overline{\kappa_{q2}}(b_{ij}\delta_{kl}+\delta_{ij}b_{kl})+2\overline{\mu_1}(\delta_{ik}a_{jl}+\delta_{il}a_{jk}+\delta_{jl}a_{ik}+\delta_{jk}a_{il})\\ &+2\overline{\mu_2}(\delta_{ik}b_{jl}+\delta_{il}b_{jk}+\delta_{jl}b_{ik}+\delta_{jk}b_{il})+\overline{\kappa_{p4}}a_{ijkl}+\overline{\kappa_{q4}}b_{ijkl}\\ &+\overline{\kappa_{s4}}(c_{ijkl}+c_{klij})\quad i,j,k,l=1,2,3\end{aligned} \tag{17}$$

where

$$\bar{k}=\langle k\rangle_S=\int_{\xi=0}^{\infty}\int_{\eta=0}^{\infty}k(\xi,\eta)\psi_S(\xi,\eta)\quad d\xi d\eta\quad [\mathrm{Pa}] \tag{18}$$

with k representing any of the material constants in (17) and $\langle\rangle_S$ brackets denoting shape averaging. We use $\langle\rangle_R$ brackets for rotation averaging and standard definition of single brackets $\langle\rangle$ indicating orientation averaging to define a_{ij} and b_{ij} as second order orientation and curvature tensors respectively:

$$a_{ij}=\langle p_ip_j\rangle=\int_{\beta=-\pi/2}^{\pi/2}\int_{\alpha=0}^{2\pi}p_ip_j\psi(\alpha,\beta)\cos\beta\ \ d\alpha d\beta\ \ i,j=1,2,3 \tag{19}$$

$$b_{ij}=\langle q_iq_j\rangle_R=\int_{\gamma=0}^{2\pi}\int_{\beta=-\pi/2}^{\pi/2}\int_{\alpha=0}^{2\pi}q_iq_j\psi_R(\alpha,\beta,\gamma)\cos\beta\ \ d\alpha d\beta d\gamma\ \ i,j=1,2,3 \tag{20}$$

Similarly, we define a_{ijkl}, b_{ijkl} and c_{ijkl} as fourth order orientation, curvature and mixed tensors:

$$\begin{aligned}a_{ijkl}&=\langle p_ip_jp_kp_l\rangle,\quad b_{ijkl}=\langle q_iq_jq_kq_l\rangle_R,\quad c_{ijkl}\\ &=\langle p_ip_jq_kq_l\rangle_R\quad i,j,k,l=1,2,3\end{aligned} \tag{21}$$

We have therefore defined all the terms in Eq. (17) that allow us to obtain the form of a stiffness tensor for a material containing curved fibers in an arbitrary configuration. The remaining task is to find nine constants for a material containing curved fibers in a single configuration. Before doing this, however, we explore the properties of the geometric configuration tensors and the character of the resulting material anisotropy.

2.6. Properties of geometric configuration tensors

In this section, we investigate properties of the second and fourth order orientation tensors a_{ij} and a_{ijkl}, the second and fourth order curvature tensors b_{ij} and b_{ijkl}, and the mixed tensor c_{ijkl}. In the absence of fiber curvature, definitions of a_{ij} and a_{ijkl} given in Eqs. (19) and (20) reduce to definitions identical to those provided by Advani and Tucker [10]. Correspondingly, all of the equations above reduce to previously developed theories. The orientation tensors are fully symmetric:

$$a_{ij}=a_{ji}\quad\text{and}\quad a_{ijkl}=a_{jikl}=a_{kijl}=a_{lijk}=a_{klij},\quad\text{etc.} \tag{22}$$

with information about second order tensor being contained within fourth order tensor and the trace of the second order tensor reducing to unity, i.e.:

$$a_{ijkk}=a_{ij},\quad a_{ii}=1 \tag{23}$$

We can write identical expressions for fully symmetric curvature tensors b_{ij} and b_{ijkl}. Full symmetry for fourth-order tensors implies 15 distinct components.

The mixed tensor is not completely symmetric. However, it is symmetric with respect to the first pair and last pair of indexes.

$$c_{ijkl}=c_{ijlk}=c_{jilk} \tag{24}$$

Thus, there are 36 unique components in c_{ijkl}. Eq. (14) imposes additional symmetry:

$$s_{ijkl}=(c_{ijkl}+c_{klij})=\langle p_ip_jq_kq_l+p_kp_lq_iq_j\rangle_R\quad i,j,k,l=1,2,3 \tag{25}$$

The tensor s_{ijkl} has the same symmetry as the elastic tensor and has 21 distinct components. We can therefore conclude that the stiffness tensor produced using configuration averaging contains the base tensor with 21 distinct components, while the stiffness tensor constructed via standard orientation averaging would contain a base tensor with only 15 distinct components corresponding to the full symmetry of a_{ijkl}.

2.7. Obtaining material parameters for a material in a single configuration

We now describe a procedure for obtaining the material parameters in Eq. (17). If a material contains fibers in a limited range of configurations, these constants could be obtained experimentally. However, such an empirical approach would be impractical for realistic DFCs. Alternatively, one could perform a large number of numerical simulations to obtain the constants.

We propose an approach based on orientation averaging and semi-empirical Halpin-Kardos [11] equations. Regarding a curved fiber in an arbitrary configuration as an assembly of segments of straight fibers, we can assign an orientation tensor to any given segment. We will first define a planar orientation tensor for a bent fiber with shape given by ξ, η in fiber coordinate system $\mathbf{f} = (\mathbf{p},\mathbf{q},\mathbf{s})$, and subsequently rotate the result to obtain the solution for arbitrary configuration. From Fig. 5, we note that $\phi = \varphi$ and $\theta = \frac{\pi}{2}$ for a segment of bent fiber with orientation given by vector $\tilde{\boldsymbol{p}}$.

The probability of finding a segment with given orientation is given by

$$\tilde{\psi}(\phi) = \begin{cases} \frac{1}{\pi\eta} & \text{for } \phi \in < -\frac{\eta}{2}, \frac{\eta}{2} > \\ 0 & \text{elswhere} \end{cases} \tag{26}$$

Components of orientation tensors $\tilde{a}_{ij}$ and $\tilde{a}_{ij}$ representing the segments of bent fiber can be calculated from definition given in Eq. (19) and (20).

$$\begin{aligned} \tilde{a}_{1111} &= \frac{3\eta + (4+\cos\eta)\sin\eta}{8\eta}, \quad \tilde{a}_{2222} \\ &= \frac{3\eta + (-4+\cos\eta)\sin\eta}{8\eta}, \tilde{a}_{1122} = \tilde{a}_{2211} = \tilde{a}_{1212} = \tilde{a}_{2112} \\ &= \tilde{a}_{2121} = \tilde{a}_{1221} = \frac{\eta - \sin\eta\cos\eta}{8\eta} \end{aligned} \tag{27}$$

with all other components reducing to zero. We now use planar orientation averaging over the transversely isotropic stiffness tensor

$$\begin{aligned} \langle \tilde{C}_{ijkl} \rangle &= \mu_s(\delta_{ik}\delta_{jl} + \delta_{il}\delta_{jk}) + \lambda_s(\delta_{ij}\delta_{kl}) + \varsigma_2(\tilde{a}_{ij}\delta_{kl} + \tilde{a}_{kl}\delta_{ij}) + (\mu_0 \\ &\quad - \mu_s)(\tilde{a}_{ik}\delta_{jl} + \tilde{a}_{il}\delta_{jk} + \tilde{a}_{jl}\delta_{ik} + \tilde{a}_{jk}\delta_{il}) + \varsigma_4\tilde{a}_{ijkl} i,j,k,l \\ &= 1,2,3 \end{aligned} \tag{28}$$

where μ_s, λ_s, μ_0, ς_2, ς_4 are material constants for straight fibers obtained from the Halpin-Kardos [11] equations and the following relations:

$$\begin{aligned} \mu = G_{23},\ \mu_0 = G_{12}, \quad \lambda &= \frac{-E_1E_2G_{23}}{E_1E_2 - 4E_1G_{23} + 4E_2G_{23}v_{12}^2} - G_{23}, \\ \varsigma_2 &= G_{23} + \frac{E_1E_2G_{23}(1-2v_{12})}{E_1E_2 - 4E_1G_{23} + 4E_2G_{23}v_{12}^2}, \\ \varsigma_4 &= G_{23} - 4G_{12} + \frac{{E_1}^2(E_2 - 4G_{23}) + E_1E_2G_{23}(4v_{12}-1)}{E_1E_2 - 4E_1G_{23} + 4E_2G_{23}v_{12}^2} \end{aligned} \tag{29}$$

The orientation averaging in Eq. (28) results in an orthotropic stiffness tensor. Consequently, we can obtain nine material constants in Eq. (14) for a material containing curved fibers:

$$\begin{aligned} \mu &= \mu_s - \varsigma_4\tilde{a}_{1122}; \lambda = \lambda_s + 2\varsigma_4\tilde{a}_{1122}; \kappa_{p2} \\ &= \varsigma_2\tilde{a}_{11} - 2\tilde{a}_{1122}\varsigma_4; \kappa_{q2} = \varsigma_2\tilde{a}_{22} - 2\tilde{a}_{1122}\varsigma_4; \mu_1 \\ &= \frac{1}{2}((\mu_0 - \mu_s)\tilde{a}_{11} + 2\tilde{a}_{1122}\varsigma_4); \mu_2 \\ &= \frac{1}{2}((\mu_0 - \mu_s)\tilde{a}_{22} + 2\tilde{a}_{1122}\varsigma_4); \kappa_4 = \tilde{a}_{1111}\varsigma_4; \kappa_{q4} \\ &= \tilde{a}_{2222}\varsigma_4; \kappa_{s4} = 3\tilde{a}_{1122}\varsigma_4 \end{aligned} \tag{30}$$

Table 1
Fiber and matrix properties from Ref. [1].

E_f [Pa]([psi])	v_f	E_m [Pa]([psi])	v_m	V_f	ξ
7.24×10^{10} (10.5×10^6)	0.2	3.45×10^9 (0.5×10^6)	0.35	0.2	100

For straight fiber with $\eta \to 0$, the limiting process reduces an orthotropic material with nine material constants to a transversely isotropic material with five material constants as expected: $\mu = \mu_s$, $\lambda = \lambda_s, \kappa_{p2} = \varsigma_2, \kappa_{p4} = \varsigma_4, \mu_1 = \frac{1}{2}(\mu_0 - \mu_s), \mu_2 = \kappa_{q2} = \kappa_{q4} = \kappa_{s4} = 0$.

It should be noted that there are many other approaches for obtaining material constants which may result in better predictions of material properties.

3. Examples

To illustrate the proposed approach, we will follow our derivation in reverse. In Table 1, we use numerical values for fiber and matrix properties given in an appendix of Ref. [10].

To generate material constants for a material with fibers in single configuration, we use the Halpin-Kardos [11] equations and Eqs. (29) and (30). Fig. 6 shows material constants in Eq. (17) as a function of curvature η for a material in with fibers single configuration.

Note that straight fibers and fibers forming half of a circle have five distinct material constants corresponding to a transversely isotropic material. The constants that will be used in later are given in Table 2.

To provide a tool for better understanding of the influence of fiber curvature on material properties, we can use the transformations listed in [13] to generate three Young's moduli E_p, E_q, E_s, shear moduli G_{pq}, G_{ps}, G_{qs} and Poisson's ratio v_{pq}, v_{ps}, v_{qs} with subscripts indicating directions in the fiber coordinate system as shown in Fig. 7.

All of the results above are obtained through orientation averaging of the transversely isotropic stiffness tensor and represent a material with fibers in a single configuration.

To demonstrate the concept of configuration averaging, we calculate geometric tensors for a material with fibers in a finite set of configurations from the following definition:

$$\begin{aligned} a_{ijkl} &= \sum_{K=1}^{N} \Upsilon_K \frac{p_ip_jp_kp_l}{Z}, b_{ijkl} = \sum_{K=1}^{N} \Upsilon_K \frac{q_iq_jq_kq_l}{Z}, s_{ijkl} \\ &= \sum_{K=1}^{N} \Upsilon_K \frac{p_ip_jq_kq_l + q_iq_jp_kp_l}{Z} \quad i,j,k,l = 1,2,3 \end{aligned} \tag{31}$$

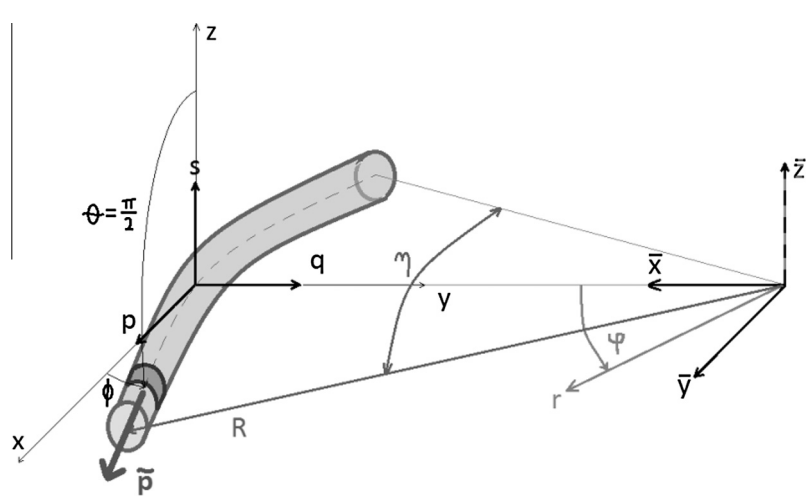

Fig. 5. Orientation vector $\tilde{p}$ for a segment of bent fiber.

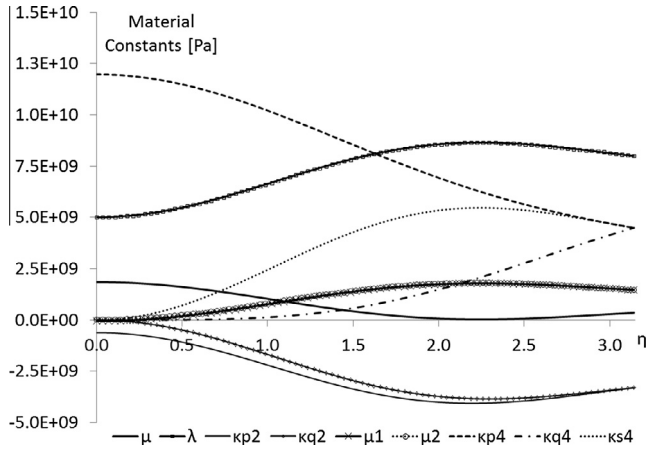

Fig. 6. Material constants as a function of curvature η for a material in with fibers single configuration having aspect ratio $\xi = 100$ and constituent properties listed in Table 1.

where $Z = \sum_{L=1}^{N} \Upsilon_L \cos B_L$ and vectors $\boldsymbol{p} = \boldsymbol{p}(A_K, B_K)$, $\boldsymbol{q} = \boldsymbol{q}(A_K, B_K, \Gamma_K)$ are calculated directly from (4) and (5). Υ_K indicates the fraction of fibers in given configuration. The second order-tensors can be obtained through contraction.

We consider a hypothetical material consisting of an ensemble of three fibers ($N = 3$) with the geometric configuration parameters listed in Table 3.

Using standard representation of symmetric fourth order tensor with symmetry given in Eq. (12) as 6×6 matrix, the configuration given in Table 1 results in the following geometric tensors:

$$a_{(4)} = \begin{bmatrix} 7.85\times10^{-1} & 6.07\times10^{-3} & 1.32\times10^{-2} & 8.44\times10^{-3} & 4.07\times10^{-2} & 3.92\times10^{-2} \\ 6.07\times10^{-3} & 7.08\times10^{-3} & 2.82\times10^{-2} & 1.41\times10^{-2} & 8.5\times10^{-3} & 4.43\times10^{-3} \\ 1.32\times10^{-2} & 2.82\times10^{-2} & 1.13\times10^{-1} & 5.64\times10^{-2} & 3.29\times10^{-2} & 1.66\times10^{-2} \\ 8.44\times10^{-3} & 1.41\times10^{-2} & 5.64\times10^{-2} & 2.82\times10^{-2} & 1.66\times10^{-2} & 8.5\times10^{-3} \\ 4.07\times10^{-2} & 8.5\times10^{-3} & 3.29\times10^{-2} & 1.66\times10^{-2} & 1.32\times10^{-2} & 8.44\times10^{-3} \\ 3.92\times10^{-2} & 4.43\times10^{-3} & 1.66\times10^{-2} & 8.5\times10^{-3} & 8.44\times10^{-3} & 6.07\times10^{-3} \end{bmatrix} \tag{32}$$

$$b_{(4)} = \begin{bmatrix} 8.55\times10^{-2} & 2.54\times10^{-2} & 2.46\times10^{-2} & -2.22\times10^{-2} & -4.58\times10^{-2} & 4.17\times10^{-2} \\ 2.54\times10^{-2} & 7.88\times10^{-1} & 9.71\times10^{-3} & 3.22\times10^{-2} & -1.53\times10^{-2} & -3.11\times10^{-2} \\ 2.46\times10^{-2} & 9.71\times10^{-3} & 7.08\times10^{-3} & -6.13\times10^{-3} & -1.32\times10^{-2} & 1.17\times10^{-2} \\ -2.22\times10^{-2} & 3.22\times10^{-2} & -6.13\times10^{-3} & 9.71\times10^{-3} & 1.17\times10^{-2} & -1.53\times10^{-2} \\ -4.58\times10^{-2} & -1.53\times10^{-2} & -1.32\times10^{-2} & 1.17\times10^{-2} & 2.46\times10^{-2} & -2.22\times10^{-2} \\ 4.17\times10^{-2} & -3.11\times10^{-2} & 1.17\times10^{-2} & -1.53\times10^{-2} & -2.22\times10^{-2} & 2.54\times10^{-2} \end{bmatrix} \tag{33}$$

$$s_{(4)} = \begin{bmatrix} 2.53\times10^{-2} & 8.1\times10^{-1} & 1.04\times10^{-1} & 8.47\times10^{-2} & 2.03\times10^{-2} & -2.28\times10^{-2} \\ 8.1\times10^{-1} & 1.94\times10^{-2} & 3.48\times10^{-2} & 9.59\times10^{-3} & 3.16\times10^{-2} & 5.29\times10^{-2} \\ 1.04\times10^{-1} & 3.48\times10^{-2} & 5.64\times10^{-2} & -1.15\times10^{-2} & -4.41\times10^{-2} & 5.25\times10^{-2} \\ 8.47\times10^{-2} & 9.59\times10^{-3} & -1.15\times10^{-2} & -2.53\times10^{-2} & -3.01\times10^{-2} & 2.38\times10^{-2} \\ 2.03\times10^{-2} & 3.16\times10^{-2} & -4.41\times10^{-2} & -3.01\times10^{-2} & -3.12\times10^{-2} & 1.91\times10^{-3} \\ -2.28\times10^{-2} & 5.29\times10^{-2} & 5.25\times10^{-2} & 2.38\times10^{-2} & 1.91\times10^{-3} & 5.84\times10^{-3} \end{bmatrix} \tag{34}$$

The reader may readily verify that Eq. (23) hold and note that the mixed tensor contains 21 distinct constants. We consider two cases of fiber shapes. In our first hypothetical material, all three of our fibers are straight ($\eta = 0$) with aspect ratio $\xi = 100$, while in the second material, the fibers are curved with $\eta = \frac{\pi}{4}$. Shape averaging of identically shaped fibers will result in constants listed in nine material constants listed in Table 2. We can now use these constants with geometric tensors listed in Eqs. (32)–(34) in Eq. (17) to assemble stiffness tensors. For the material with straight fibers:

$$\mathrm{C} = \begin{bmatrix} 1.7\times10^{10} & 4.56\times10^{9} & 4.57\times10^{9} & 5.24\times10^{7} & 4.28\times10^{8} & 4.25\times10^{8} \\ 4.56\times10^{9} & 8.73\times10^{9} & 5.22\times10^{9} & 1.12\times10^{8} & 5.12\times10^{7} & 9.61\times10^{6} \\ 4.57\times10^{9} & 5.22\times10^{9} & 9.84\times10^{9} & 6.18\times10^{8} & 3.35\times10^{8} & 1.62\times10^{8} \\ 5.24\times10^{7} & 1.12\times10^{8} & 6.18\times10^{8} & 2.18\times10^{9} & 1.96\times10^{8} & 9.75\times10^{7} \\ 4.28\times10^{8} & 5.12\times10^{7} & 3.35\times10^{8} & 1.96\times10^{8} & 1.96\times10^{9} & 9.69\times10^{7} \\ 4.25\times10^{8} & 9.61\times10^{6} & 1.62\times10^{8} & 9.75\times10^{7} & 9.69\times10^{7} & 1.88\times10^{9} \end{bmatrix} \tag{35}$$

and for the material with curved fibers:

$$\mathrm{C} = \begin{bmatrix} 1.61\times10^{10} & 4.99\times10^{9} & 4.6\times10^{9} & 9.2\times10^{7} & 4.18\times10^{8} & 3.47\times10^{8} \\ 4.99\times10^{9} & 8.74\times10^{9} & 5.16\times10^{9} & 1.16\times10^{8} & 8.86\times10^{7} & 9.06\times10^{7} \\ 4.6\times10^{9} & 5.16\times10^{9} & 9.81\times10^{9} & 5.38\times10^{8} & 2.3\times10^{8} & 1.41\times10^{8} \\ 9.2\times10^{7} & 1.16\times10^{8} & 5.38\times10^{8} & 2.14\times10^{9} & 1.74\times10^{8} & 1.31\times10^{8} \\ 4.18\times10^{8} & 8.86\times10^{7} & 2.3\times10^{8} & 1.74\times10^{8} & 1.97\times10^{9} & 1.34\times10^{8} \\ 3.47\times10^{8} & 9.06\times10^{7} & 1.41\times10^{8} & 1.31\times10^{8} & 1.34\times10^{8} & 2.32\times10^{9} \end{bmatrix} \tag{36}$$

It is apparent that for the material containing straight fibers, configuration averaging recovers the results of orientation averaging and results in a stiffness tensor with 15 distinct constants for a_{ijkl}. Configuration averaging of curved fibers generally gives a stiffness tensor with 21 distinct constants corresponding to anisotropy of s_{ijkl}. Our particular method for obtaining material constants through orientation averaging of fibers with identical length is equivalent with segmental orientation averaging, however modified methods will result in stiffness tensor with symmetry given in Eq. (12).

Table 2
Orthotropic material constants for a material with curved fibers in single configuration given by shape parameters $\xi = 100$ for straight fiber $\eta = 0$ and curved fiber with $\eta = \frac{\pi}{4}$.

η	μ (Pa)	λ (Pa)	κ_{p2} (Pa)	κ_{q2} (Pa)	μ_1 (Pa)	μ_2 (Pa)	κ_{p4} (Pa)	κ_{q4} (Pa)	κ_{s4} (Pa)
0	1.85×10^9	5.00×10^9	-6.17×10^8	0	-5.28×10^7	0	1.20×10^{10}	0	0
$\frac{\pi}{4}$	1.31×10^9	6.09×10^9	-1.67×10^8	-1.12×10^9	2.22×10^8	2.69×10^8	1.08×10^{10}	5.29×10^7	1.63×10^9

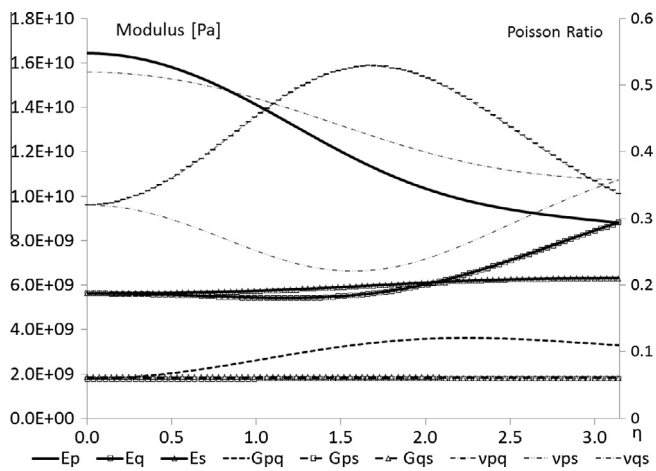

Fig. 7. Engineering constants as a function of curvature η for a material in with fibers single configuration having aspect ratio $\xi = 100$ and constituent properties listed in Table 1.

Table 3
Geometric configuration parameters for three fibers.

	A_K	B_K	Γ_K	Υ_K
Fiber 1 ($K = 1$)	0	0	0	1/3
Fiber 2 ($K = 2$)	$\pi/32$	$\pi/32$	$\pi/32$	1/3
Fiber 3 ($K = 3$)	$\pi/3$	$\pi/3$	$\pi/3$	1/3

Now we consider a material in which the fiber rotation is perfectly random over the entire range of angles α, β and γ. This distribution is represented by a constant function

$$\psi_R(\alpha,\beta,\gamma) = \frac{1}{8\pi^2}, \quad \alpha\langle\in 0,2\pi\rangle, \beta \in \left\langle -\frac{\pi}{2}, \frac{\pi}{2}\right\rangle, \gamma\langle\in 0,2\pi\rangle \tag{37}$$

And with the help of symbolic equation solver [15], the geometric tensors can be obtained analytically by performing integration as outlined in Eqs. (19)–(21).

$$a_{(4)} = \begin{bmatrix} \frac{1}{5} & \frac{1}{15} & \frac{1}{15} & 0 & 0 & 0 \\ \frac{1}{15} & \frac{1}{5} & \frac{1}{15} & 0 & 0 & 0 \\ \frac{1}{15} & \frac{1}{15} & \frac{1}{5} & 0 & 0 & 0 \\ 0 & 0 & 0 & \frac{1}{15} & 0 & 0 \\ 0 & 0 & 0 & 0 & \frac{1}{15} & 0 \\ 0 & 0 & 0 & 0 & 0 & \frac{1}{15} \end{bmatrix} \tag{38}$$

$$b_{(4)} = \begin{bmatrix} \frac{1}{5} & \frac{1}{15} & \frac{1}{15} & 0 & 0 & 0 \\ \frac{1}{15} & \frac{1}{5} & \frac{1}{15} & 0 & 0 & 0 \\ \frac{1}{15} & \frac{1}{15} & \frac{1}{5} & 0 & 0 & 0 \\ 0 & 0 & 0 & \frac{1}{15} & 0 & 0 \\ 0 & 0 & 0 & 0 & \frac{1}{15} & 0 \\ 0 & 0 & 0 & 0 & 0 & \frac{1}{15} \end{bmatrix} \tag{39}$$

$$s_{(4)} = \begin{bmatrix} \frac{2}{15} & \frac{4}{15} & \frac{4}{15} & 0 & 0 & 0 \\ \frac{4}{15} & \frac{2}{15} & \frac{4}{15} & 0 & 0 & 0 \\ \frac{4}{15} & \frac{4}{15} & \frac{2}{15} & 0 & 0 & 0 \\ 0 & 0 & 0 & -\frac{1}{15} & 0 & 0 \\ 0 & 0 & 0 & 0 & -\frac{1}{15} & 0 \\ 0 & 0 & 0 & 0 & 0 & -\frac{1}{15} \end{bmatrix} \tag{40}$$

The reader may verify that changing the magnitude of fiber curvature does not influence the resulting stiffness tensor with material constants as calculated above. For example, both sets of constants in Table 2 result in the same stiffness tensor:

$$C = \begin{bmatrix} 1.06\times10^{10} & 5.39\times10^{9} & 5.39\times10^{9} & 0 & 0 & 0 \\ 5.39\times10^{9} & 1.06\times10^{10} & 5.39\times10^{9} & 0 & 0 & 0 \\ 5.39\times10^{9} & 5.39\times10^{9} & 1.06\times10^{10} & 0 & 0 & 0 \\ 0 & 0 & 0 & 2.61\times10^{9} & 0 & 0 \\ 0 & 0 & 0 & 0 & 2.61\times10^{9} & 0 \\ 0 & 0 & 0 & 0 & 0 & 2.61\times10^{9} \end{bmatrix} \tag{41}$$

Our particular method of obtaining orthotropic material constants by orientation averaging of transversely isotropic stiffness tensor only accounts for changing orientation along the axis of the curved fiber and ensures that we obtain identical stiffness tensors regardless of fiber curvature. In general, the method of configuration averaging would result in different stiffness tensors for varying fiber curvature, however the form of the stiffness tensor would not change. It is clear that this material is isotropic with Young's modulus $E = 6.99 \times 10^9$ Pa and Poisson's ratio $\nu = 3.37 \times 10^{-1}$.

We have therefore established that changing the magnitude of fiber curvature in a material with fibers in a single configuration has significant influence on the stiffness tensor, while perfectly random fiber architecture negates the effects of fiber curvature.

4. Comparison with experiments

Now we compare results of our method to against a realistic material produced with a common production technique. A polyamide 6,6 (PA6,6) material containing 50% of glass fibers by weight in the form of 12 mm long pulltruded pellets was injection molded into an edge-gated plaque cavity of 600 mm × 600 mm and 2.8 mm thickness. The physical samples used in this study were harvested from the centers of these plaques. Fig. 8 shows weight-based fiber length distribution in the sample obtained by pyrolysis and measurements of a digitized image of 2000 individual glass filaments [5].

A nominal diameter of 15 μm was measured for glass fibers in these samples using optical microscopy.

Experiments were performed using an X-ray micro-tomography unit with a tensile testing machine [16]. This setup allows us to perform tomography at the beginning of the experiment and obtain fiber orientation as well as fiber curvature measurements. After reconstructing the sample cross-section slices with a Feldkamp's cone beam convolution-backprojection algorithm [17], the fibers appear as bright circular features in each slice. A Hough Transform [18] is used to detect the circular fibers at each slice and the recursive nearest neighbor algorithm searches the sample volume to connect each fiber through neighbor slices. Note that

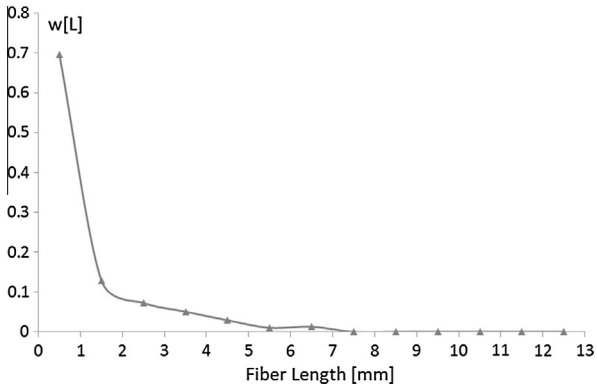

Fig. 8. Weight-based experimentally measured fiber length distribution.

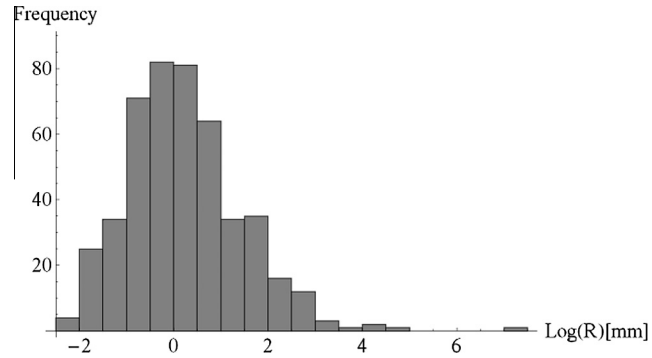

Fig. 9. Histogram of fiber curvature radius measured using X-ray micro-tomography.

cross-section images needs to be generated for all the major axes (i.e., x, y, z axes) in order to segment fibers in all directions. Finally, a segmented fiber is represented as points in 3D space. To determine the orientation of the fiber, the points eignevectors and eignevalues provide the direction and the magnitude of the point spread, respectively. Consequently, the first and second largest latent vectors give the orientation of the fiber. Although by empirical observation of the processed samples 45 point samples were enough to determine the orientation of the fiber, in order to reduce the impact of noise in the reconstructed slices, the fibers considered in this paper have a minimum of 75 point samples. After projecting the segmented fiber to a 2D plane, by aligning the mayor eigenvectors with the plane axes, an optimal solution is found by fitting a circle to the points with the standard Levenberg-Marquardt geometrical scheme [19] – the initial point is given by approximating the fiber curvature radius and center with Taubin's fitting algorithm [20]. Measurements were performed on segments of 466 fibers with the best reconstruction. Although it is theoretically possible to obtain configuration of each individual filament using the setup presented in [16], the reduced field of view and imperfect alignment of the testing machine in the tomography unit produces artifacts making tracking of each fiber difficult. Fig. 9 shows a histogram of the fiber curvature radius measured confirming the presence of curved fibers.

Note that a glass fiber subjected to pure bending can have a minimum fiber curvature radius of approximately 147 μm and fibers with a radius exceeding kilometers are essentialy straight fibers with an infinite radius of fiber curvature.

Eqs. (11)–(13) provide the following geometric tensors calculated based on measured filaments.

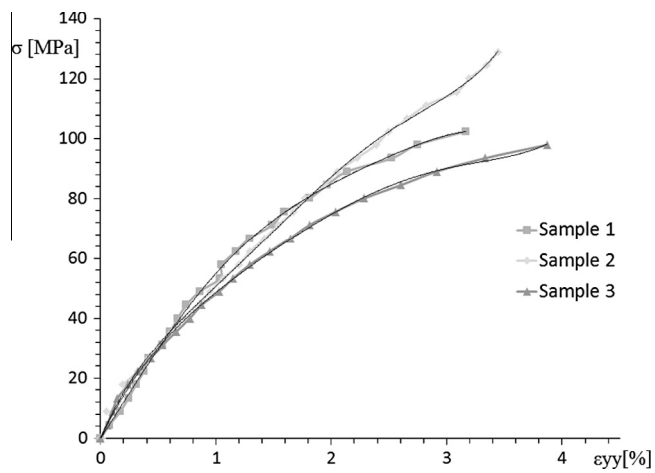

Fig. 10. Stress–strain curves from digital image correlation.

Table 4
Zero strain tangential Young's moduli from digital image correlation of X-ray images of loaded samples.

	Sample 1	Sample 2	Sample 3	Average
E (GPa)	8.88	5.84	8.09	7.61

$$a_{(4)} = \begin{bmatrix} 8.62\times10^{-2} & 1.38\times10^{-2} & 1.07\times10^{-1} & -2.79\times10^{-3} & -3.21\times10^{-2} & 9.66\times10^{-3} \\ 1.38\times10^{-2} & 3.27\times10^{-2} & 1.13\times10^{-2} & -1.4\times10^{-3} & -2.94\times10^{-3} & 4.02\times10^{-3} \\ 1.07\times10^{-1} & 1.13\times10^{-2} & 6.17\times10^{-1} & 1.27\times10^{-3} & -1.27\times10^{-1} & 4.28\times10^{-3} \\ -2.79\times10^{-3} & -1.4\times10^{-3} & 1.27\times10^{-3} & 1.13\times10^{-2} & 4.28\times10^{-3} & -2.94\times10^{-3} \\ -3.21\times10^{-2} & -2.94\times10^{-3} & -1.27\times10^{-1} & 4.28\times10^{-3} & 1.07\times10^{-1} & -2.79\times10^{-3} \\ 9.66\times10^{-3} & 4.02\times10^{-3} & 4.28\times10^{-3} & -2.94\times10^{-3} & -2.79\times10^{-3} & 1.38\times10^{-2} \end{bmatrix} \tag{42}$$

$$b_{(4)} = \begin{bmatrix} 1.43\times10^{-1} & 9.96\times10^{-2} & 2.42\times10^{-2} & -7.95\times10^{-3} & 2.24\times10^{-2} & -1.27\times10^{-2} \\ 9.96\times10^{-2} & 5.08\times10^{-1} & 3.29\times10^{-2} & -2.35\times10^{-2} & 2.35\times10^{-2} & -5.42\times10^{-2} \\ 2.42\times10^{-2} & 3.29\times10^{-2} & 3.54\times10^{-2} & -1.44\times10^{-3} & 9.26\times10^{-3} & -3.74\times10^{-3} \\ -7.95\times10^{-3} & -2.35\times10^{-2} & -1.44\times10^{-3} & 3.29\times10^{-2} & -3.74\times10^{-3} & 2.35\times10^{-2} \\ 2.24\times10^{-2} & 2.35\times10^{-2} & 9.26\times10^{-3} & -3.74\times10^{-3} & 2.42\times10^{-2} & -7.95\times10^{-3} \\ -1.27\times10^{-2} & -5.42\times10^{-2} & -3.74\times10^{-3} & 2.35\times10^{-2} & -7.95\times10^{-3} & 9.96\times10^{-2} \end{bmatrix} \tag{43}$$

$$s_{(4)} = \begin{bmatrix} 7.17\times10^{-2} & 1.59\times10^{-1} & 2.43\times10^{-1} & -7.25\times10^{-3} & -2.48\times10^{-2} & -1.22\times10^{-2} \\ 1.59\times10^{-1} & 2.77\times10^{-2} & 5.12\times10^{-1} & -7.27\times10^{-4} & -1.06\times10^{-1} & 8.34\times10^{-3} \\ 2.43\times10^{-1} & 5.12\times10^{-1} & 7.33\times10^{-2} & -2.79\times10^{-2} & 2.36\times10^{-2} & -4.89\times10^{-2} \\ -7.25\times10^{-3} & -7.27\times10^{-4} & -2.79\times10^{-2} & -1.46\times10^{-2} & 3.87\times10^{-3} & 1.14\times10^{-3} \\ -2.48\times10^{-2} & -1.06\times10^{-1} & 2.36\times10^{-2} & 3.87\times10^{-3} & -5.87\times10^{-2} & 2.86\times10^{-2} \\ -1.22\times10^{-2} & 8.34\times10^{-3} & -4.89\times10^{-2} & 1.14\times10^{-3} & 2.86\times10^{-2} & -1.31\times10^{-2} \end{bmatrix} \tag{44}$$

Mechanical tests were performed on double dog-bone shoulder loaded samples with 1 mm × 1 mm cross section [21]. Fig. 10 shows stress–strain curves from the digital image correlation using X-ray images of sample deformed under known load.

The solid lines in Fig. 10 show fifth order polynomial least square fit that provide zero strain tangential Young's modulus values summarized in Table 4.

Table 5 shows constituent material properties used for prediction of the stiffness tensor. The matrix properties were obtained by averaging the zero strain tangential modulus of five PA6,6 samples containing resin identical to that used in the reinforced material.

Averaging for a material with fibers in finite set of configurations was used with the number of fibers $N = 466$. A random number generator in Mathematica [15] was used to select values from fiber length measurements and pair them with radii to generate values for ξ and η for each filament since we could not measure both fiber length and the magnitude of fiber curvature with a single physical method. Due to the small sample size, the fiber length distribution was influenced significantly by machining the edges of the sample and reducing filament lengths. The values of ξ for each filament were adjusted by randomly generating the intersection of the fiber with the sample and eliminating portions of the filament outside of the sample which was removed during machining of the sample. Two stiffness tensors were calculated for one hundred randomly selected sets of 466 fibers. One stiffness tensor accounted for fiber curvature, while the other was calculated with the assumption of straight fibers. Fig. 11 shows sample stiffness Ec for curved fibers and Es for straight fibers. The assumption of curved fibers resulted in mean sample stiffness prediction of 8.77 GPa, while the mean for straight fiber prediction was 9.05 Gpa.

Table 5
Constituent Material Properties for Injection Molded PA6,6 Containing 50% Glass Fibers By Weight.

E_f (Pa)	ν_f	E_m (Pa)	ν_m	V_f
7.24×10^{10}	0.2	2.63×10^{9}	0.35	0.31

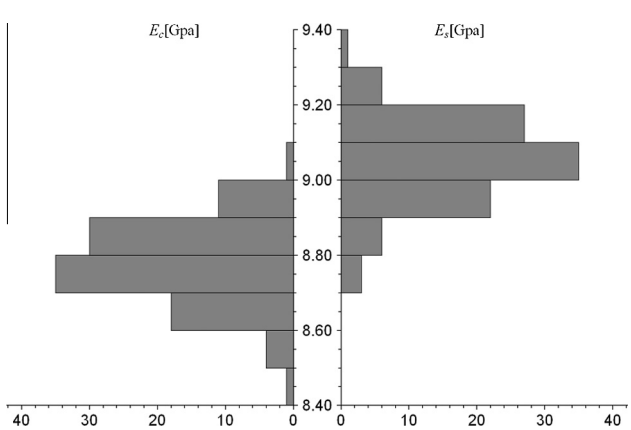

Fig. 11. Predicted sample Young's moduli Ec and Es for curved fibers and straight fibers respectively.

The deviation from the average experimental measurement is therefore 15% for a model with curved fibers and 19% for a model with straight fibers. It is likely that we would obtain a closer match if we accounted for time dependent or non-linear behavior of the matrix material. Accounting for visco-elastic effects would allow us to calculate the first few points along the stress strain curve obtained with a difficult experimental technique [16]. It should also be noted that we have not performed any calibration of matrix material properties or any other arbitrary adjustments of parameters that are often performed in engineering practice.

5. Conclusions

A new practical method for obtaining the stiffness tensor for discontinuous fiber composite materials containing curved fibers has been introduced, as well as a new concept for curved fiber configuration that is described by five dimensionless parameters. Two parameters describe the fiber shape and three parameters describe the rotation of that shape with respect to the laboratory coordinate system. Furthermore, an ensemble of fibers is described by a configuration distribution function. For a system of non-interacting fibers, separation of variables is used to define the configuration distribution function as a product of shape distribution and rotation configuration functions. Additionally, we have proposed a new method of configuration averaging for constructing a stiffness tensor for a material containing an ensemble of curved fibers. This configuration averaging led to the definitions of orientation, curvature, and mixed fourth order tensors. The anisotropic stiffness tensor for an ensemble of curved fibers was then assembled using these three tensors and nine averaged elastic constants. We have provided a method for predicting these material constants and have shown that the method of configuration averaging reduces to orientation averaging if all fibers within the material remain straight. We have also presented numerical examples and have concluded that the impact of fiber curvature on stiffness tensor properties depends on the rotation distribution function of the DFC material. Finally, we compared results of configuration averaging and orientation averaging using experimentally obtained data. X-ray micro-tomography was used to obtain fiber orientation and curvature parameters, while X-ray digital image correlation was used to obtain stress–strain behavior of injection molded material. We demonstrated that configuration averaging produces a closer match to the experimental results than orientation averaging.

Acknowledgements

The authors would like to express gratitude to the American Chemistry Council, Plastics Division for supporting research and innovation in this area.

References

[1] Lei HF, Zhang ZQ, Liu B. Effect of fiber arrangement on mechanical properties of short fiber reinforced composites. Compos Sci Technol 2012;72(4):506–14.

[2] Tu ST et al. Numerical simulation of saturation behavior of physical properties in composites with randomly distributed second-phase. J Compos Mater 2005;39(7):617–31.

[3] Thomason JL, Vlug MA. Influence of fibre length and concentration on the properties of glass fibre-reinforced polypropylene. 1. Tensile and flexural modulus. Compos A – Appl Sci Manuf 1996;27(6):477–84.

[4] Thomason JL, Vlug MA. Influence of fibre length and concentration on the properties of glass fibre-reinforced polypropylene. 4. Impact properties. Compos A – Appl Sci Manuf 1997;28(3):277–88.

[5] Kunc V, Frame BJ, Nguyen BN, Tucker III CL, Velez-Garcia G. Fiber length distribution measurement for long glass and carbon fiber reinforced injection molded thermoplastics. In: Composites conference and exposition, society of plastic engineers. Troy, Michigan; 2007.

[6] Clarke AR, Davidson N, Archenhold G. A multitransputer image analyzer for 3d-fiber orientation studies in composites. Trans Roy Microscop Soc: New Ser 1990;1:305–8.

[7] Bay RS, Tucker CL. Stereological measurement and error-estimates for 3-dimensional fiber orientation. Polym Eng Sci 1992;32(4):240–53.

[8] ASTM, D2584-11. Standard test method for ignition loss of cured reinforced resins. West Conshohocken, PA; 2011.

[9] ASTM, D3171-11. Standard test methods for constituent content of composite materials. West Conshohocken, PA; 2011.

[10] Advani SG, Tucker CL. The use of tensors to describe and predict fiber orientation in short fiber composites. J Rheol 1987;31(8):751–84.

[11] Halpin JC, Kardos JL. Strength of discontinuous reinforced composites. 1. Fiber reinforced composites. Polym Eng Sci 1978;18(6):496–504.

[12] Chadwick P, Vianello M, Cowin SC. A new proof that the number of linear elastic symmetries is eight. J Mech Phys Solids 2001;49(11):2471–92.

[13] Lubarda VA, Chen MC. On the elastic moduli and compliances of transversely isotropic and orthotropic materials. J Mech Mater Struct 2008;3(1):153–71.

[14] Spencer AJM. The formulation of constitutive equation for anisotropic solids. In: Boehler JP, editor. Mechanical behavior of anisotropic solids. The Hague: Martinus Nijhoff Publishers; 1982. p. 2–26.

[15] Wolfram Research, I. Mathematica Edition: Version 7.0. Champaign, Illinois Wolfram Research Inc.; 2008

[16] Kunc V. Observation of composite materials using coupled mechanical testing and computed tomography. In: SEM XI international congress and exposition on experimental and applied mechanics. Orlando, FL; 2008.

[17] Feldkamp LA, Davis LC, Kress JW. Practical cone-beam algorithm. J Opt Soc Am A 1984;1(6):612–9.

[18] Illingworth J, Kittler J. A survey of the hough transform. Comput Vision, Graph, Image Process 1988;44(1):87–116.

[19] Moré J. The levenberg-marquardt algorithm: implementation and theory. In: Numerical analysis, lecture notes in mathematics. Berlin, Heidelberg: Springer; 1978.

[20] Taubin G. Estimation of planar curves, surfaces and nonplanar space curves defined by implicit equations, with applications to edge and range image segmentation. IEEE Trans PAMI 1991;13:1115–38.

[21] Kunc V. Tensile specimen design and experimental procedures for characterizing polymeric composites using X-ray based micro-tomography, in SAMPE-ASC. Memphis, TN; 2008.